Available online at www.sciencedirect.com
ScienceDirect
Journal of Power Sources 159 (2006) 914–921
JOURNAL OF POWER SOURCES
www.elsevier.com/locate/jpowsour

Fuel cell studies of perovskite-type materials for IT-SOFC

J. Peña-Martínez [a,b], D. Marrero-López [b], J.C. Ruiz-Morales [b], B.E. Buergler [a], P. Núñez [b,*], L.J. Gauckler [a,**]

[a] *Nonmetallic Inorganic Materials, Department of Materials, ETH-Zurich, Switzerland*
[b] *Inorganic Chemistry Department, University of La Laguna, Tenerife, Spain*

Received 26 July 2005; received in revised form 8 November 2005; accepted 9 November 2005
Available online 20 December 2005

Abstract

The electrochemical performance of solid oxide fuel cells (SOFCs) based on perovskite-type materials (ABO_3) was investigated. $La_{0.9}Sr_{0.1}Ga_{0.8}Mg_{0.2}O_{3-\delta}$ (LSGM) ceramics were used as electrolyte and a composite containing $La_{0.8}Sr_{0.2}MnO_3$ (LSM) as cathode. $Ba_{0.5}Sr_{0.5}Co_{0.8}Fe_{0.2}O_{3-\delta}$ (BSCF) was also used as cathode and $La_{0.75}Sr_{0.25}Cr_{0.5}Mn_{0.5}O_{3-\delta}$ (LSCM) as anode materials. Furthermore, fluorite-type $Sm_{0.15}Ce_{0.85}O_{2-\delta}$ (SDC) material was used as buffer layer between the electrolyte and the anode to avoid possible interfacial reactions. The maximum power density value of BSCF/LSGM/LSCM with 1.5 mm thick electrolyte supported cell was 160 mW cm^{-2} at 1073 K, using moist H_2 diluted with N_2 as fuel and air as oxidant.

Keywords: Perovskite-type oxides; Electrochemical performance; Solid oxide fuel cell; $Ba_{0.5}Sr_{0.5}Co_{0.8}Fe_{0.2}O_{3-\delta}$; $La_{0.75}Sr_{0.25}Cr_{0.5}Mn_{0.5}O_{3-\delta}$; $La_{0.9}Sr_{0.1}Ga_{0.8}Mg_{0.2}O_{3-\delta}$

1. Introduction

The versatile perovskite-type structure (ABO_3) is an interesting option to develop new materials for intermediate temperature solid oxide fuel cells (IT-SOFCs). It is well known that the ionic conductivity of $La_{0.9}Sr_{0.1}Ga_{0.8}Mg_{0.2}O_{2.85}$ (LSGM) [1–5] is higher as compared to yttria-doped zirconia (YSZ) at intermediate temperatures (773–1073 K). This material has an ionic conductivity of about 0.1 S cm^{-1} at 1073 K, good chemical stability and negligible electronic conduction over a broad range of oxygen partial pressures (1–10^{-20} atm) [6]. On the other hand, LSGM has some disadvantages as electrolyte, such as undesired segregation of impurities during its synthesis, e.g. $LaSrGa_3O_7$ and $LaSrGaO_4$ [7], and chemical incompatibility with Ni-based anode materials [8,9]. Ni reacts with LSGM to form $LaNiO_3$ [10]. However, the synthesis can be optimized to reduce undesired phases and alternative anode material without nickel or a buffer layer, between electrolyte and Ni-based anode, can be used to avoid interfacial reactions [11].

Results from LSGM electrolyte supported cells with $La_{0.8}Sr_{0.2}MnO_3$ (LSM) as cathode and $La_{0.75}Sr_{0.25}Cr_{0.5}Mn_{0.5}O_{3-\delta}$ (LSCM) [12,13] as anode were reported in a previous work [14]. Dense LSGM samples were prepared by tape casting. The power density reached a value of 570 mW cm^{-2} at 1073 K with moistened H_2 and O_2 as oxidant. However, the output power density drastically decreased at 873 K, mainly due to the high polarization resistance of LSM and higher ohmic losses of the electrolyte. Therefore, different strategies were envisaged to improve the performance of LSGM-based cells using LSCM as anode material at low temperature: reducing the electrode overpotential and avoiding the possible interfacial reactions between the electrodes and the electrolyte.

For the first option, a composite of LSM and LSGM in a 30–70% molar ratio (LSM–LSGM) was used. A lower cathodic overpotential had been reported using LSM–LSGM as composite than with LSM only, both on LSGM electrolyte [15]. In addition, the recently proposed $Ba_{0.5}Sr_{0.5}Co_{0.8}Fe_{0.2}O_{3-\delta}$ (BSCF) material was used in this study as alternative cathode, due to the good properties for electrochemical reduction of oxygen in the range of 773–973 K [16]. For the second option,

* Corresponding author. Tel.: +34 922 318501; fax: +34 922 318461.
** Corresponding author. Tel.: +41 1 632 3760; fax: +41 1 632 1132.
E-mail addresses: pnunez@ull.es (P. Núñez), ludwig.gauckler@mat.ethz.ch (L.J. Gauckler).

0378-7753/$ – see front matter © 2005 Elsevier B.V. All rights reserved.
doi:10.1016/j.jpowsour.2005.11.036

$Sm_{0.15}Ce_{0.85}O_{2-\delta}$ (SDC) was used as buffer layer between the electrolyte and the anode material.

LSM/LSGM/LSCM, LSM/LSGM/SDC/LSCM, LSM–LSGM/LSGM/LSCM and BSCF/LSGM/LSCM cells were prepared and tested in this work and their performances compared.

2. Experimental

2.1. Electrodes and electrolyte preparation

LSGM electrolyte, LSM–LSGM cathode and LSCM anode materials were prepared by conventional solid state reaction, using powders of La_2O_3 (Fluka, 99.98%), Ga_2O_3 (Fluka, 99.99%), MgO (Fluka, 99%), $SrCO_3$ (Aldrich, 99.9%), Mn_2O_3 (Aldrich, 99.999%) and Cr_2O_3 (ABCR, 99.999%). La_2O_3 and MgO were fired at 1273 K for more than 3 h before weighing to remove water and impurities, in order to ensure the correct stoichiometry. Commercial powders of LSM obtained via combustion spray pyrolysis (SSC Inc. Worthingtong, USA, 99.9%) were used to prepare the LSM cathode specimens.

BSCF cathode and SDC interlayer materials were prepared via sol–gel, using powders of $Ba(NO_3)_2$ (Fluka, 99.95%), $Sr(NO_3)_2$ (Fluka, 99%), $Co(NO_3)_2{\cdot}6H_2O$ (Fluka, 98%), $Fe(NO_3)_3{\cdot}9H_2O$ (Merck, 99%), $Sm(NO_3)_3{\cdot}6H_2O$ (Alfa Aesar, 99.9%) and $Ce(NO_3)_3{\cdot}6H_2O$ (Alfa Aesar, 99.9%).

The ceramic route was done by ball-milling stoichiometric quantities of the reagents with acetone. The resulted mixture was dried and fired in air up to 1173 K for 10 h and ground again. Dense samples of LSGM were obtained by uniaxial pressing into a disk at 140 MPa, for 5 min (Ø = 3.0 cm) of the synthesized powders and sintered at 1673 K for 6 h. LSCM and LSM–LSGM powders were obtained after treatment at 1373 K for 10 h and 1473 K for 6 h, respectively.

The sol–gel route was carried out, using citric acid and ethylendiaminetetraacetic acid (EDTA) as complex agents to prepare BSCF and SDC materials. Stoichiometric cation solution of the corresponding nitrates was prepared with distilled water. An ammonium solution of EDTA, 1.5 wt.% in excess, with a ratio ligand/metal (L/M) = 1 was added. Afterwards, the citric acid solution, 1.5 wt.% in excess and in a ratio L/M = 1 and 2/3 for trivalent and divalent cations, respectively, was also added. The pH was adjusted up to 9 with addition of ammonia solution (20%, v/v). A gel was formed with continuous stirring and low heating (∼338 K). It was dried at room temperature for more than 8 h. The dried gels were fired at 573 K for 30 min.

The obtained powders were ground in an agate mortar and fired in air at 923 and 723 K for BSCF and SDC, respectively, during 5 h, ground again and finally fired at 1173 K for 5 h in air.

Electrode slurries were prepared with ethyl cellulose as binder and diethyleneglycol monobutyleter acetate as solvent. The composition (wt.%) of the slurries was 75% of electrode powders, 5% of binder and 20% of solvent.

2.2. Material characterization

X-ray diffraction (XRD) patterns were recorded using a Siemens D5000 with $K\alpha_1$ copper radiation wavelength of 0.15406 nm. The scans were performed in the 2θ range (5–120°) with 0.02° step and 10 s $step^{-1}$. XRD studies were also carried out to investigate the chemical compatibility of the electrolyte with the electrodes. Powder mixtures of LSGM with BSCF, LSGM with SDC and LSCM with SDC, 1:1 (wt.%) were ground in agate mortar and fired at 1173 and 1473 K for 10 h.

The morphology and composition of ceramic materials were observed by scanning electron microscopy (SEM) (JEOL JSM-6300 and LEO 1530) and energy dispersive X-ray spectroscopy (EDS) (NORAN Vantage) before and after the tests.

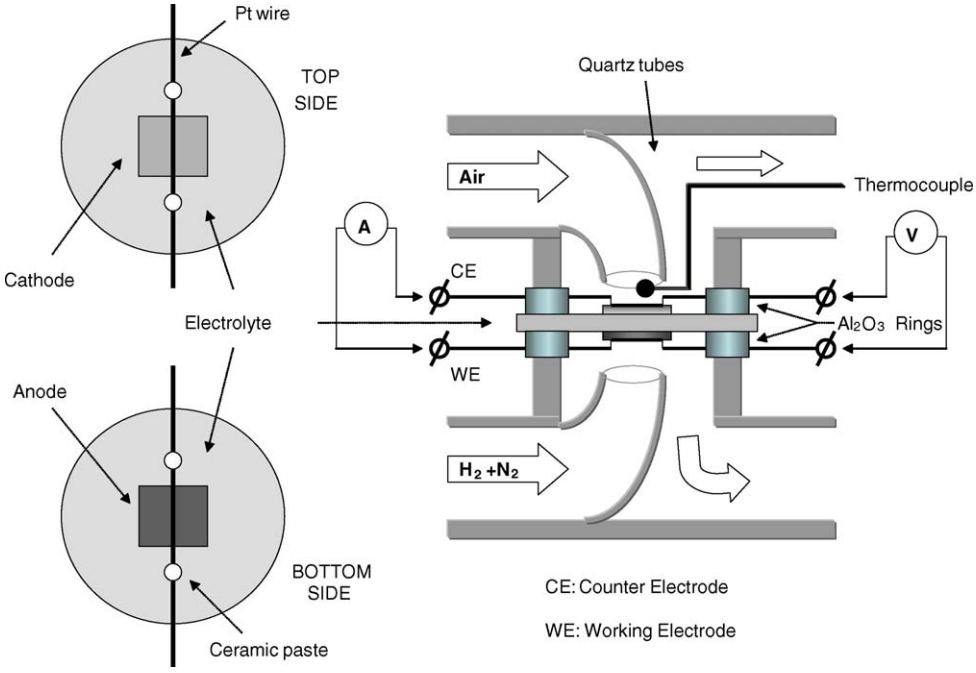

Fig. 1. Scheme of the setup for fuel cell tests.

TG/DTA studies were carried out with a STA 449 C Jupiter NETZSCH (TG/DTA) to determine the correct stoichiometry of the nitrates used in the synthesis and to estimate the optimal temperature of crystallization on powder precursors obtained by sol–gel route.

2.3. Fuel cell tests

Fuel cell tests were performed with a moistened (3% water) gas mixture of H_2 (40 vol%) and N_2 as fuel and air as oxidant. Different electrolyte supported cells were investigated: LSM/LSGM/LSCM, LSM/LSGM/SDC/LSCM, LSM–LSGM/LSGM/LSCM and BSCF/LSGM/LSCM.

The electrodes and the buffer layer were deposited via screen printing (∼50 μm thickness and 1 cm^2 of surface) using the corresponding slurry and fired at 1273–1573 K in air for 1 h. Platinum paste and mesh were used as current collector. The electrolyte-pellet dimensions were about 1.5 and 20 mm in thickness and diameter for all the cells. The measurement setup consisted of two quartz tubes for the gas transport to the electrodes (Fig. 1). The cell was mounted between two Al_2O_3 spacer rings and adjusted between the quartz tubes. High fuel and air gas flows were necessary (300 ml/min on each side at a pressure of 1 atm) due to the unsealed arrangement to obtain high values of OCV. The entire setup was heated in a tubular furnace and the temperature was varied between 873 and 1073 K. The electrochemical analyses were performed with a Zahner IM6 potentiostat.

Two-electrode configuration was used to obtain *I–V* plots, total overpotential and electrode ohmic loss. The fuel cell performance was recorded at a scan rate of 5 mV s^{-1} and the impedance of the electrochemical cell was acquired at open circuit voltage (OCV), with a frequency ranging between 0.1 Hz and 1 MHz and 20 mV of ac amplitude, obtaining reproducible spectra.

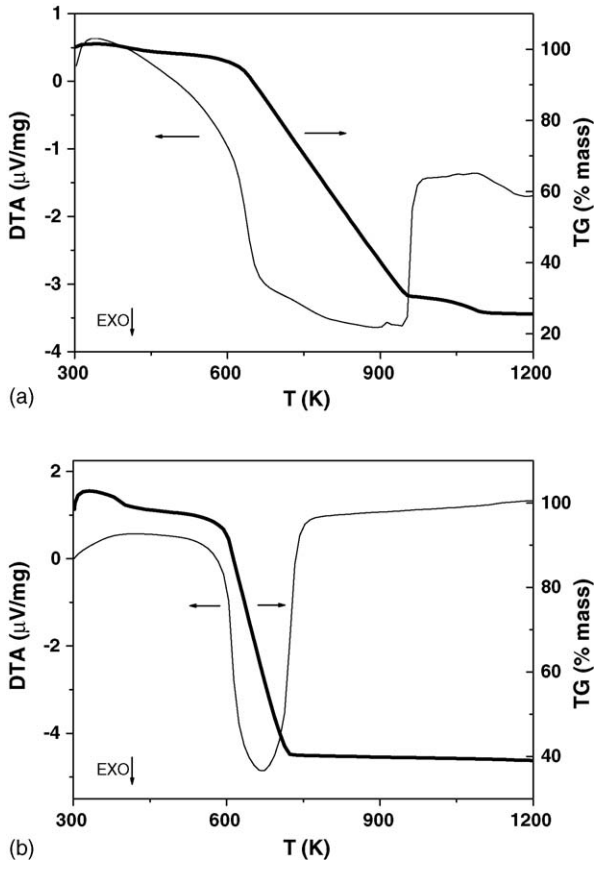

Fig. 2. TG/DTA curves of the dried precursor obtained by sol–gel route for: (a) BSCF and (b) SDC.

3. Results and discussion

3.1. BSCF and SDC characterization

TG/DTA in air for BSCF and SDC precursors are shown in Fig. 2. It can be observed that no mass loss occurs above 1073

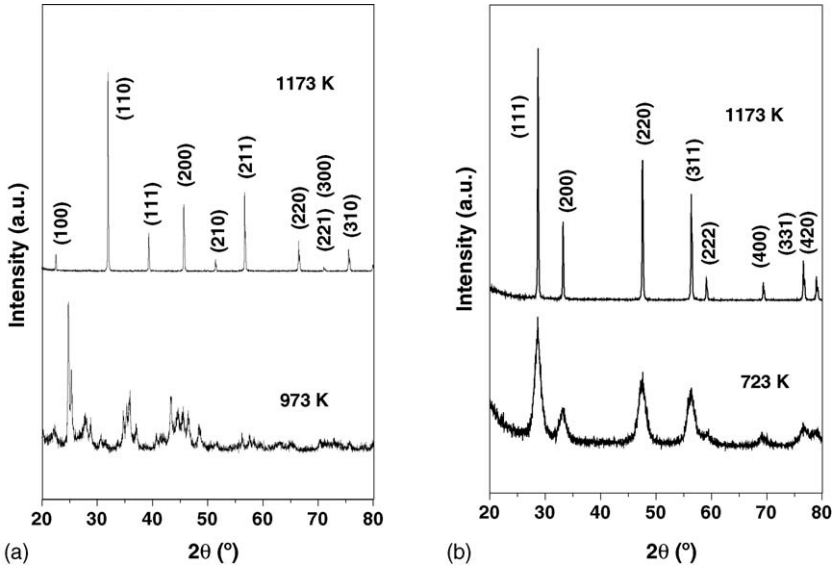

Fig. 3. Thermal evolution of XRD patterns of: (a) BSCF and (b) SDC obtained both by sol–gel route.

and 723 K for BSCF and SDC, respectively. According with these results, BSCF and SDC precursor gels were calcined. Final synthesis temperature was 1173 K in both cases. The thermal evolution of XRD patterns is shown in Fig. 3, showing single phases at 1173 and 723 K for BSCF and SDC, respectively.

BSCF and SDC patterns were refined, using FullProff and WinPlotr programs [17,18], in a symmetric cubic system with space groups *Pm3m* and *Fm3m*, and cell parameters $a = 3.9810(8)$ and 5.4289(5) Å, for BSCF and SDC, respectively.

3.2. Chemical compatibility

XRD patterns at room temperature, 1173 and 1473 K of the binary-mixed systems LSGM/BSCF, LSGM/SDC and LSCM/SDC are shown in Figs. 4–6, respectively. LSGM/LSM and LSCM/LSGM compatibility were studied in a previous work [14] and certain reactivity was found between LSGM and LSM at temperature above 1173 K and between LSGM and LSCM at 1623 K, however only LSGM/LSCM interface showed by SEM a possible cross-diffusion of Cr, Mn or La [9,19]. For this reason, the use of the SDC material as buffer layer was studied. No additional diffraction peaks were found in the LSGM/SDC (Fig. 5) and LSCM/SDC (Fig. 6) systems between room temperature and 1173 K, and neither in the BSCF/LSGM mixed system.

Two small additional peaks, identified as La_2O_3, were observed in the LSGM/SDC system (Fig. 5e) and one (unknown) in the LSCM/SDC system (Fig. 6e) for the samples fired at 1473 K. The XRD pattern of the LSGM/BSCF system at 1473 K showed only peaks of a perovskite phase, indicating the total reaction between the LSGM and BSCF phases to a new one (Fig. 4e).

Therefore, it seems there are not any chemical incompatibility between the pairs LSGM/BSCF, LSCM/SDC and LSGM/SDC at intermediate temperature (873–1073 K). It indicates that SDC material can avoid the likely interfacial reaction between LSCM anode and LSGM electrolyte at this temperature. In fact, SEM images of the electrode–electrolyte interfaces after fuel cell testing (Fig. 7) did not show any diffusion zone or any reaction. Furthermore, the three layers of the LSCM/SDC/LSGM system can be distinguished (Fig. 7e).

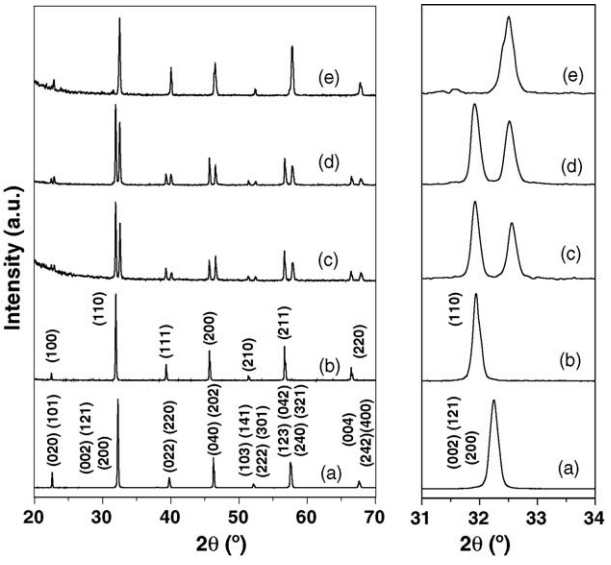

Fig. 4. XRD patterns of: (a) LSGM, (b) BSCF, (c) mixture of LSGM and BSCF at room temperature, (d) LSGM + BSCF at 1173 K and (e) LSGM + BSCF at 1473 K.

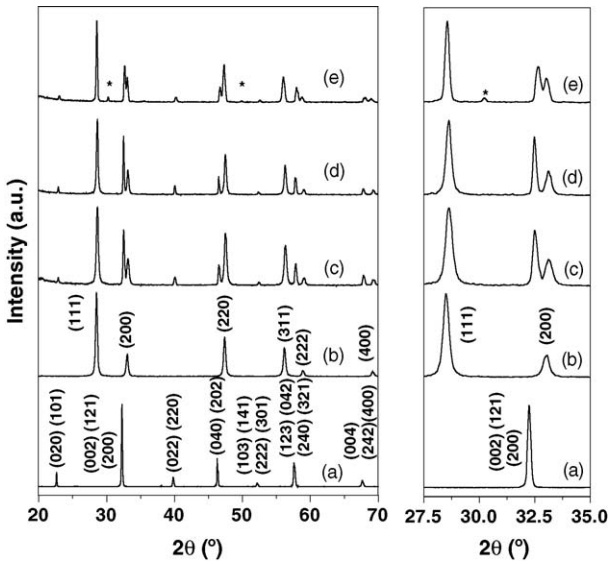

Fig. 5. XRD patterns of: (a) LSGM, (b) SDC, (c) mixture of LSGM and SDC at room temperature, (d) LSGM + SDC at 1173 K and (e) LSGM + SDC at 1473 K. Additional peaks identified as La_2O_3 (*).

However, the BSCF electrode material could be affected and seriously react with the LSGM electrolyte above 1373 K. Thus, this value was the maximum temperature used for sintering the BSCF electrode on the LSGM electrolyte.

3.3. Electrochemical characterization

3.3.1. Electrolyte and electrode resistances

The impedances of the cells were measured under asymmetric atmospheres at open circuit conditions. These impedance

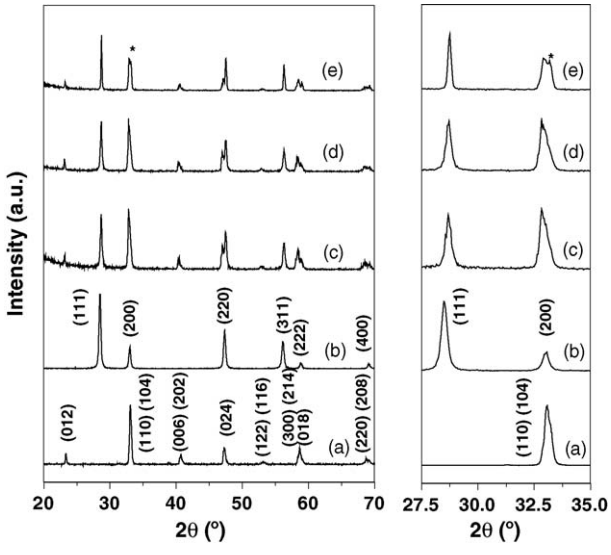

Fig. 6. XRD patterns of: (a) LSCM, (b) SDC, (c) mixture of LSCM and SDC at room temperature, (d) LSCM + SDC at 1173 K and (e) LSCM + SDC at 1473 K. Additional peak, not identified (*).

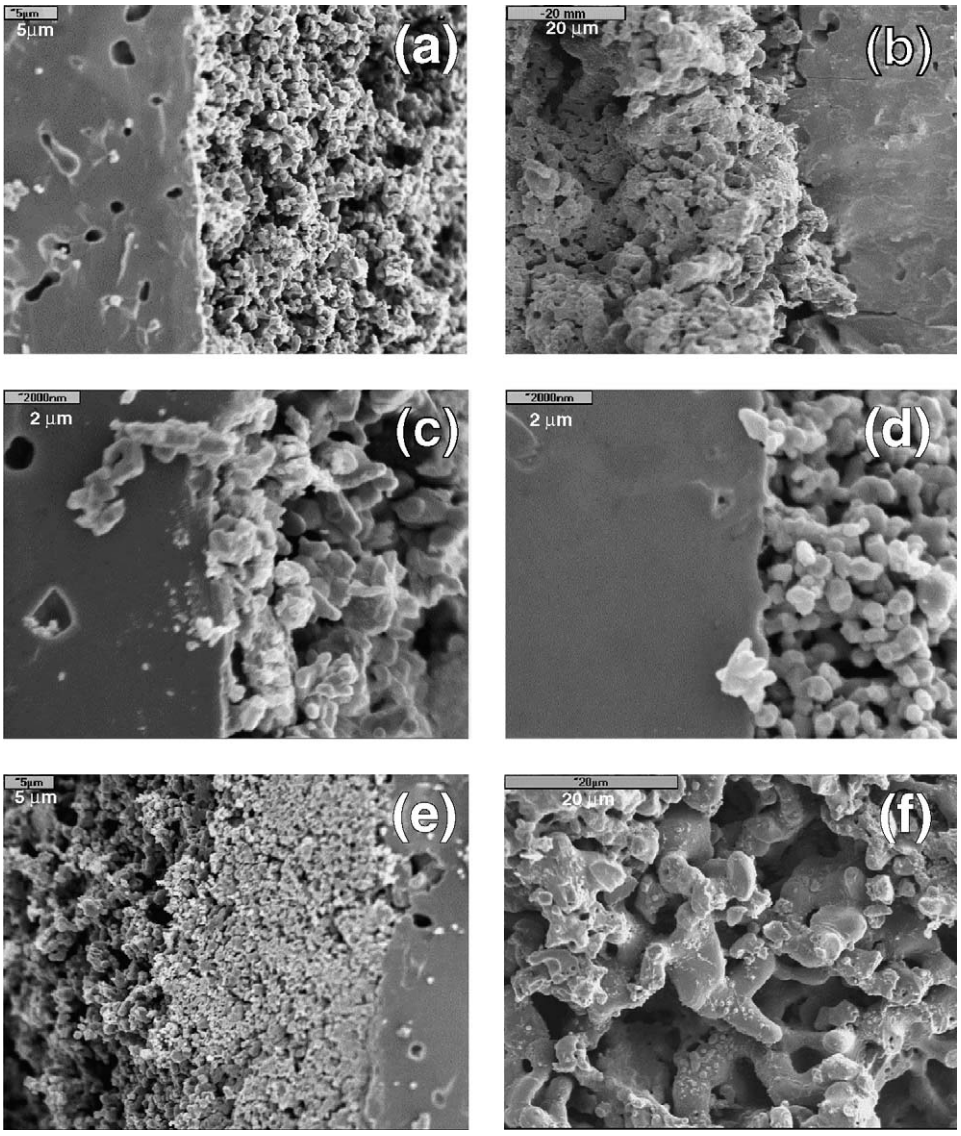

Fig. 7. SEM images of the cells after testing. Cross-sections of: (a) LSGM/LSCM, (b) BSCF/LSGM, (c) LSGM/LSM–LSGM, (d) LSGM/LSM and (e) LSCM/SDC/LSGM interfaces. (f) SEM image of BSCF surface. The electrode materials were previously sintered for 1 h at the indicated temperature: BSCF/LSGM, 1273 K; SDC/LSGM, LSM–LSGM/LSGM and LSM/LSGM, 1473 K; LSCM/LSGM and LSCM/SDC/LSGM, 1573 K.

spectra (Fig. 8) were fitted with equivalent circuits [20]. Three serial (RC) elements and a series resistance were used as equivalent circuit to fit the impedance data, except for LSM/LSGM/LSCM and BSCF/LSGM/LSCM system at 1073 K where only two serial (RC) elements and a series resistance were used, i.e. the electrolyte contribution (the series resistance) and the cathode and anode contribution (two serial (RC) circuits). Electrolyte resistances were approximately the same for LSM/LSGM/SDC/LSCM, LSM/LSGM/LSCM and BSCF/LSGM/LSCM systems (see Table 1).

The value of the electrolyte resistance (R_s) of LSM–LSGM/LSGM/LSCM is higher than those of the three other systems studied at 873 and 1073 K, and it was probably due to the reaction between LSGM and LSM in the

Table 1
Series (R_s) and polarization (R_p) resistances of the different cells at 873 and 1073 K

Fuel cell system	1073 K		873 K	
	R_s (Ω cm)	R_p (Ω cm^2)	R_s (Ω cm)	R_p (Ω cm^2)
BSCF/LSGM/LSCM	7.53	0.75	31.33	4.47
LSM/LSGM/LSCM	8.93	1.64	32.66	86.85
LSM–LSGM/LSGM/LSCM	14.13	13.73	53.20	248.29
LSM/LSGM/SDC/LSCM	8.40	25.15	39.13	156.27

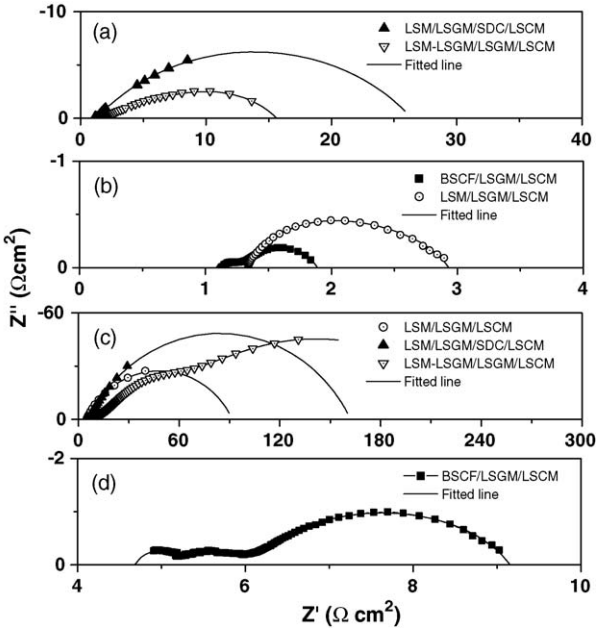

Fig. 8. Impedance spectra of the different cells at: 1073 K (a and b) and 873 K (c and d). The solid line is the fitted result obtained with equivalent circuits.

preparation of the composite via co-calcination. On the other hand, the highest polarization resistance (R_p) at 1073 K corresponded to the LSM/LSGM/SDC/LSCM system and this could be consequence of the effect of the SDC buffer layer. The polarization resistances were obtained with extrapolated data of the fitted impedance spectra. Nevertheless, the polarization resistances of the LSM/LSGM/LSCM, LSM–LSGM/LSGM/LSCM and LSM/LSGM/SDC/LSCM systems at 873 K are not enough reliable. It is obvious that the lowest values were obtained for the BSCF/LSGM/LSCM cell, 7.53 Ω cm and 0.75 Ω cm^2 for R_s and R_p, respectively, at 1073 K. When the operational temperature was decreased to 873 K the R_s and R_p resistances increase to 31.33 Ω cm and 4.47 Ω cm^2, respectively.

3.3.2. Power density

The same configuration, two-probe method, was used to obtain *I–V* plots, using humidified mixture of pure H_2 in N_2 as fuel and air as oxidant. The highest maximum power density of 160 mW cm^{-2} at 1073 K was reached with the system BSCF/LSGM/LSCM and this represents about 20% more of the maximum power density of the system LSM/LSGM/LSCM at the same temperature. Furthermore, this difference is increased up to 43% at 873 K. The others systems, LSM/LSGM/SDC/LSCM and LSM–LSGM/LSGM/LSCM, did not to reach 50% of the value obtained with the corresponding BSCF/LSGM/LSCM configuration (Fig. 9).

I–V curves of LSM/LSGM/SDC/LSCM and LSM–LSGM/LSGM/LSCM cells showed a drastical drop of the cell voltage at low current density which became less pronounced at larger current. This strong drop of the potential could be related to a high activation polarization loss.

The use of a SDC buffer layer do not help to improve the electrochemical performance of the LSGM based cell with LSCM

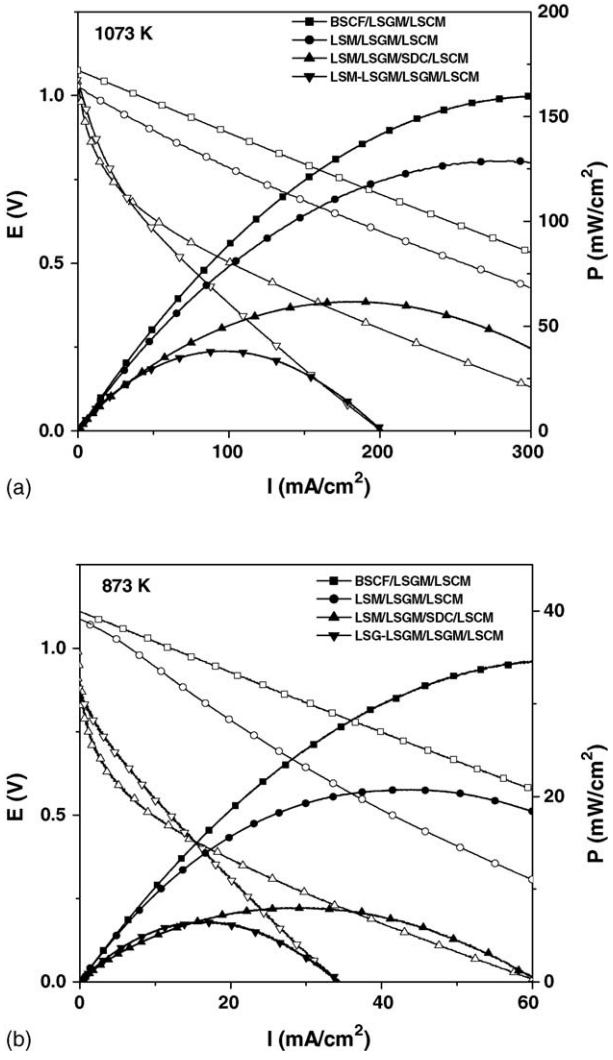

Fig. 9. Current–voltage characteristics at: (a) 1073 K and (b) 873 K.

as anode material. In fact, the maximum power density of the LSM/LSGM/LSCM system is about 50 and 60% at 1073 and 873 K, respectively, higher than that of the buffered system LSM/LSGM/SDC/LSCM. This result does not follow the trend proposed by Tao and Irvine [13] using $Ce_{0.8}Gd_{0.2}O_{2-\delta}$ (GDC) buffer layer between YSZ/LSCM systems; where they found that the anode polarization resistance could be further decreased if a thin layer of GDC is deposited between YSZ electrolyte and LSCM anode. These authors suggested the combination of LSCM and GDC as anode material. However, Huang and Goodenough [11] used a thin buffer layer of SDC (∼10 μm) placed between a NiO-composite anode and a LSGM electrolyte to avoid the reaction between Ni and LSGM to give rise a lanthanum–nickel oxide. Furthermore, at the anode in a reducing atmosphere Ce^{3+} is partially formed increasing the electronic conductivity. The system Ce^{4+}/Ce^{3+} helps the oxidation of the fuel and the ionic transport across this layer. Goodenough and coworkers [21] have also reported the use of a thin film of $La_{0.4}Ce_{0.6}O_{2-\delta}$ (LDC) as a buffer between LSGM electrolyte and NiO–LDC anode composite. They concluded that the LDC buffer layer successfully prevented the formation of undesired

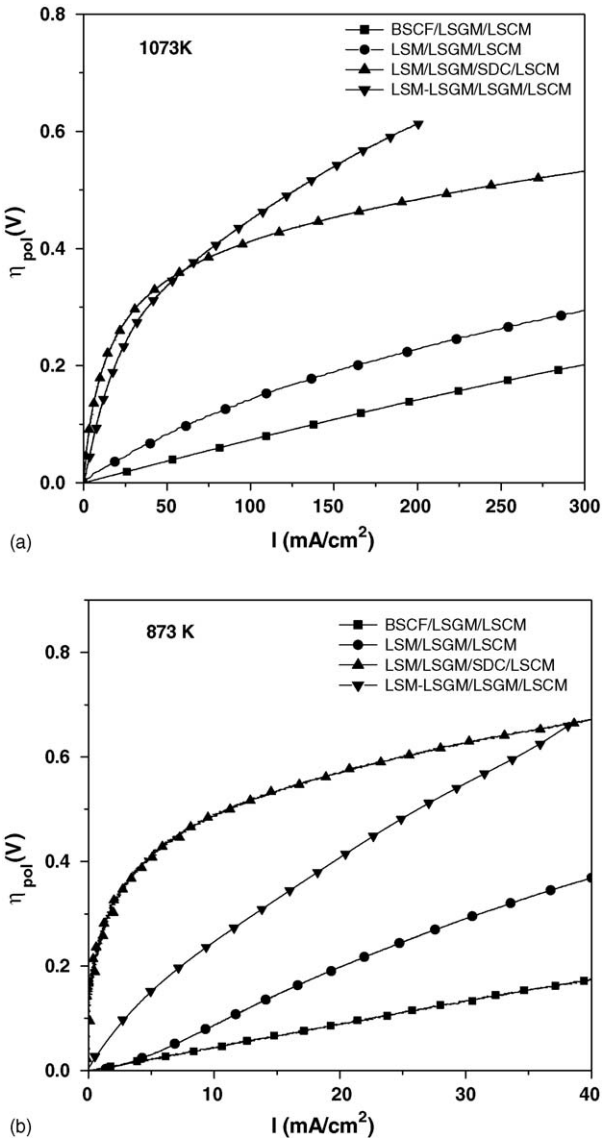

Fig. 10. Electrode overpotentials of the different cells at: (a) 1073 K and (b) 873 K.

phases. In our case, more studies on the effect of SDC layer between LSGM and LSCM materials are now under investigation to clarify its influence on the electrochemical performance of the LSGM based cells.

3.3.3. Electrode overpotentials

Fig. 10 compares the overall electrode overpotentials in a single-cell configuration at 873 and 1073 K. The lowest value of overpotential corresponded to the BSCF/LSGM/LSCM system. For example, the overpotential of this system at 300 mA cm^{-2} and 1073 K is 2.6 times lower than the value of LSM/LSGM/SDC/LSCM system and 1.45 times lower than the value of LSM/LSGM/LSCM. The shape of the overpotential–current density curve in BSCF-cell was practically linear in the current density range studied, with a slope of 0.6 V cm^2 A^{-1}. However, the others showed a non-linear trace. LSM–LSGM/LSGM/LSCM and LSM/LSGM/SDC/LSCM also had high overpotential even at lower values of current density.

The lowest value of overpotential obtained for the BSCF/LSGM/LSCM system compared with LSM/LSGM/LSCM system could be attributed to the low activation overpotential of cobaltite-based cathodes. In this sense, Huang et al. [9] found similar results comparing $SrCo_{0.8}Fe_{0.2}$ (SCF) with $La_{0.85}Sr_{0.15}MnO_3$ as cathode materials and both on doped $LaGaO_3$ (LGO) electrolytes, explaining this behavior in terms of a high oxygen flux of the cobalt-containing perovskite [22].

The LSM–LSGM composite was used as cathode material instead of LSM in order to reduce the cathodic overpotential. Yi and Choi found a lower cathodic overpotential using this kind of composite than using only LSM, both on LGO-based electrolyte [23]. It was reported that it is more important to reduce the cathodic overpotential and the reaction between electrode and electrolyte than the control of the microstructure. In our case, it should be noted that the electrode overpotential of LSM–LSGM/LSGM/LSCM is higher than for LSM/LSGM/LSCM at 873 and 1073 K (Fig. 10a and b). In this study, a large difference between the LSM/LSGM (Fig. 7d) and LSM–LSGM/LSGM interface (Fig. 7c) was observed. The microstructure of LSM appears to be more porous than the LSM–LSGM. This corresponds to the better performance of the LSM/LSGM/LSCM than LSM–LSGM/LSGM/LSCM in the current-voltage characteristics at 873 and 1073 K (see Fig. 9a and b). In addition, the shape of the voltage–current curve at low values of current density of LSM–LSGM/LSGM/LSCM system compared with LSM/LSGM/LSCM indicates a high activation polarization loss possibly due to the higher activation energy for the oxygen reduction. Definitively, the obtained power density of the LSM–LSGM/LSGM/LSCM cell at 873 and 1073 K (Fig. 9a and b), suggested that the use of LSM–LSGM composite prepared by co-calcination instead of LSM as cathode with LSGM as electrolyte and LSCM as anode is not a possibly solution to increase the obtained electrochemical performance of the LSM/LSGM/LSCM system at low temperature (873 K) [14].

Comparing the use of different alternative cathodes, BSCF system showed the best overpotential, resistance and power density. For this reason, it seems advisable to study in depth in a future work the system BSCF/LSGM/LSCM with thin electrolyte layer. In addition, it can be seen in Fig. 7b and d a large difference in the microstructure and morphology of BSCF and LSM. LSM material possesses a better structure than BSCF, but worse overpotential. Thus, according to Yi and Choi, it is probably more important in LSGM electrolyte-based cells to reduce electrode overpotential than to control the electrode microstructure to increase the electrochemical performance at intermediate temperatures.

4. Conclusions

Current–potential, current power density, electrode and electrolyte resistances and overpotential of the LSM–LSGM/LSGM/LSCM, LSM/LSGM/SDC/LSCM, LSM/LSGM/LSCM and BSCF/LSGM/LSCM cells were investigated in this study at

1073 and 873 K, using moistened hydrogen–nitrogen mixtures as fuel and air as oxidant.

The lowest electrode overpotential, highest power density and lowest polarization resistance values were obtained for BSCF/LSGM/LSCM system, i.e. 160 mW cm^{-2} at 1073 K with 1.5 mm thickness electrolyte, $R_s = 7.53\ \Omega$ cm and $R_p = 0.75\ \Omega$ cm^2. The use of a SDC buffer layer between LSGM electrolyte and LSCM anode material do not help to improve the electrochemical performance of the LSM/LSGM/LSCM cell, neither using a LSM–LSGM composite prepared via co-calcination instead of LSM cathode material.

Acknowledgements

The authors acknowledge financial support from Spanish Research Program (MAT-2001-3334 and MAT-2004-03856) and Canary Islands Government (COFI 2002-027, Ph.D. and ETH sojourn grants).

References

[1] T. Ishihara, H. Matsuda, Y. Takita, J. Am. Chem. Soc. 116 (1994) 3801–3803.
[2] K. Huang, S.R. Tichy, J.B. Goodenough, J. Am. Chem. Soc. 81 (1998) 2565–2575.
[3] T. Ishihara, H. Matsuda, M. Azni, Y. Takita, Solid State Ionics 86–88 (1996) 197–201.
[4] P.R. Slater, J.T.S. Irvine, T. Ishihara, Y. Takita, J. Solid State Chem. 139 (1998) 135–143.
[5] J.H. Kim, H.I. Yoo, Solid State Ionics 140 (2001) 105–113.
[6] O. Yamamoto, Electrochim. Acta 45 (2000) 2423–2435.
[7] A. Matraszek, L. Singheiser, D. Kobertz, K. Hilpert, M. Miller, O. Schulz, M. Martin, Solid State Ionics 166 (2004) 343–350.
[8] M. Guillodo, P. Vernoux, J. Fouletier, Solid State Ionics 127 (2000) 99–107.
[9] K. Huang, J. Wan, J.B. Goodenough, J. Electrochem. Soc. 148 (2001) A788–A794.
[10] K. Huang, M. Feng, J.B. Goodenough, C. Milliken, J. Electrochem. Soc. 144 (1997) 3620.
[11] K. Huang, J.B. Goodenough, J. Alloy. Compd. 303–304 (2000) 454–464.
[12] S. Tao, J.T.S. Irvine, Nat. Mater. 2 (2003) 320–323.
[13] S. Tao, J.T.S. Irvine, J. Electrochem. Soc. 151 (2004) A252–A259.
[14] J. Peña-Martínez, D. Marrero-López, J.C. Ruiz-Morales, C. Savaniu, J.T.S. Irvine, P. Núñez, Chem. Mater., submitted for publication.
[15] J.Y. Yi, G.M. Choi, J. Eur. Ceram. Soc. 24 (2004) 1359–1363.
[16] Z. Shao, S.M. Haile, Nature 431 (2004) 170–173.
[17] J. Rodríguez-Carvajal, FullProf Suite, Laboratoire Léon Brillouin, CEA-Saclay, France, 2004.
[18] T. Roisnel, J. Rodríguez-Carvajal, WinPlotr, Laboratoire Léon Brillouin-LCSI, France, 2004.
[19] S. Tao, J.T.S. Irvine, J.A. Kilner, Adv. Mater. 17 (2005) 1734–1737.
[20] D. Johnson, Zview Program, Version 2.8, Scribner Associates, Inc., Southern Pines, North Carolina, 1990–2002.
[21] J.-H. Wan, J.-Q. Yan, J.B. Goodenough, J. Electrochem. Soc. 152 (2005) A1511–A1515.
[22] K. Huang, J.B. Goodenough, J. Electrochem. Soc. 148 (2001) E203.
[23] J.Y. Yi, G.M. Choi, Solid State Ionics 175 (2004) 145–149.